

Received: 2018.02.11  
Accepted: 2018.05.02  
Published: 2018.05.17

# 5-Hydroxy-4'-Nitro-7-Propionyloxy-Genistein Inhibited Invasion and Metastasis via Inactivating Wnt/ $\beta$ -Catenin Signal Pathway in Human Endometrial Carcinoma Ji Endometrial Cells

Authors' Contribution:  
Study Design A  
Data Collection B  
Statistical Analysis C  
Data Interpretation D  
Manuscript Preparation E  
Literature Search F  
Funds Collection G

ABCDEF **Jun Bai**  
AFG **Xin Luo**

Department of Obstetrics and Gynecology, The First Clinical School of Jinan University, Guangzhou, Guangdong, P.R. China

**Corresponding Author:** Xin Luo, e-mail: [tluox@jnu.edu.cn](mailto:tluox@jnu.edu.cn)

**Source of support:** The present study was supported by a grant from the First Clinical School of Jinan University (No. FRPR201601-04)

**Background:** Chemotherapy has been assuring more important roles in the treatment of carcinoma. Developing new types of drugs with less adverse effects and low drug resistance has become an important researching focus. The present study aimed to investigate the anticancer effects of 5-hydroxy-4'-nitro-7-propionyloxy-genistein (HNPG) and to elucidate its underlying molecular mechanism.


**Material/Methods:** The inhibitory effects of cell viability of HNPG were detected using 3-(4,5-dimethyl-2-thiazolyl)-2,5-diphenyl-2-H-tetrazolium bromide (MTT) assay, flat plate clone formation method, and Transwell assay. The distribution of cell cycle was analyzed using flow cytometry (FCM) method. The morphological alteration, root-mean-squared roughness (Rq), average roughness (Ra), Young's modulus, and adhesive force were measured by atomic force microscope (AFM) assay. Quantitative real-time polymerase chain reaction (qRT-PCR) and Western blot analysis were used to explore the possible molecular mechanism.

**Results:** We found that HNPG had dramatic activity against Ji Endometrial cells (JEC) *in vitro*, inhibited the proliferation and colony formation, attenuated invasion and migration ability, and arrested cell cycle in G1 phase, all in a dose-dependent manner. Simultaneously, cell bodies shrunk, pseudopod structures retracted, Rq and Ra were reduced, and Young's modulus and adhesive force increased, accompanied by downregulation of  $\beta$ -catenin, C-Myc, Cyclin D1, matrix metalloprotease 2 (MMP-2), matrix metalloprotease 7 (MMP-7), and matrix metalloprotease 9 (MMP-9).

**Conclusions:** HNPG dramatically inhibited invasion and metastasis of JEC cells *in vitro*. Its molecular mechanism might be related to inactivation of the wnt/ $\beta$ -catenin signal pathway, accumulated cells in G1/S phase, inhibited cell proliferation, improved adhesive force between cells, and reduced cell plasticity and elasticity.

**MeSH Keywords:** **beta Catenin • Neoplasm Invasiveness • Neoplasm Metastasis**

**Full-text PDF:** <https://www.medscimonit.com/abstract/index/idArt/909472>

 5499

 1

 7

 35



## Background

Endometrial carcinoma (EC) is a group of epithelial malignancies that occur in the endometrium. Endometrial adenocarcinoma is the most common form, accounting for 80–90% of all pathological types [1]. EC is one of the 3 malignant tumors of the female genital tract, accounting for 7% of malignant tumors in human carcinomas, and 20–30% of female malignant tumors [2]. The average age of people with EC is 60 years and 75% of patients are aged 50 years or older. The morbidity of EC has been increasing worldwide in recent years [3]. The main treatment methods of EC include surgery, radiotherapy, chemotherapy, and hormone therapy [1,2]. Chemotherapy is one of the most important treatment measures for EC of late-stage and recurrence, and it can also be used for EC patients with high-risk factors of recurrence [1,3]. Chemotherapy drugs such as cisplatin, paclitaxel, cyclophosphamide, fluorouracil, mitomycin, and etoposide are commonly used in clinical chemotherapy [4]. Although chemotherapy has assumed an increasingly important role in the treatment of EC, the generation of drug resistance and its adverse effects restrict its clinical use. Therefore, developing new types of drug with low adverse effects or without adverse effects and low drug resistance has become an important research focus.

Genistein (GEN), an isoflavone extracted from soybeans, was reported to possess extensive antitumor activities via regulating oncogenes in many signal pathways, such as anti-proliferation, inhibitive metastasis, and induction of apoptosis [5]. However, the lower absorption rate in the gastrointestinal tract and lower biological activity have limited its clinical use [6]. It is well known that structural modification can enhance solubility and biological activity [7]. 5-hydroxy-4'-nitro-7-propionyloxy-genistein (HNPG), a novel synthetic derivative of GEN, possesses a nitro group in C-4', a hydroxyl group at C-5, and a propionyloxy group at C-7 [8,9], which means that HNPG possesses more solubility and biological activity than its precursor, GEN. It was reported that HNPG inhibits proliferation in gastric and breast cancer, but its antitumor effect has not been examined in EC, and its molecular biological mechanism has not been investigated [8,9]. The JEC cell line, in which estrogen receptor expression is negative, was used to investigate the pharmacological effect of phytoestrogens and their molecular mechanisms in the ER cell signal pathway [10,11].

The wnt/ $\beta$ -catenin signal pathway is a complex and conservative signal pathway in mammals. It is composed of a series of interacting proteins, regulates cell proliferation, adhesion, movement and so on, plays an important role in embryo development and tissue repair [12,13]. Abnormal activation of wnt/ $\beta$ -catenin signal pathway can cause abnormal proliferation and differentiation and result in tumor occurrence [12]. In addition, wnt/ $\beta$ -catenin signal pathway may induce the

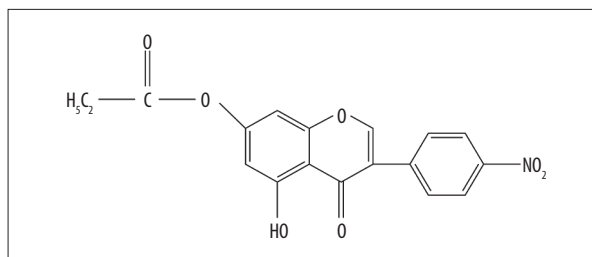


**Figure 1.** Chemical structure of 5-hydroxy-4'-nitro-7-propionyloxy-genistein.

process of epithelial mesenchymal transformation (EMT) and affect the progression and metastasis of carcinoma [13]. The wnt/ $\beta$ -catenin signal pathway plays an important role in the occurrence of EC, and about 40% of EC cases exhibit abnormal activation of the wnt/ $\beta$ -catenin signal pathway, especially in endometrial adenocarcinoma (EEC) [14]. Researchers discovered that the mutation of CT-NNB1 exon-3 can cause  $\beta$ -catenin protein accumulation and activated wnt/ $\beta$ -catenin signal pathways [15]. It was reported that the expression of wnt10b was significantly increased in EC tissues and the PCDH10-wnt/ $\beta$ -catenin-MALAT1 signal pathway is involved in the occurrence and progression of EC [16,17].

In the present study, the anticancer effects of HNPG in JEC cells were evaluated *in vitro*, and the results demonstrated that HNPG inhibits proliferation, clone formation, invasion, and metastasis, which might be attributed to HNPG increasing the cell accumulation in G1/S phase, altering cell morphological features, decreasing Rq and Ra, enhancing Young's modulus and adhesive force in JEC cells through inactivating the wnt/ $\beta$ -catenin signal pathway, and downregulating  $\beta$ -catenin, C-Myc, Cyclin D1, MMP-2, MMP-7, and MMP-9, which not only demonstrates the antitumor effects of HNPG, but also highlights the basic molecular biological mechanism of HNPG compared with previous reports [8,9].

## Material and Methods

### Materials

5-hydroxy-4'-nitro-7-propionyloxy-genistein (HNPG) and genistein (GEN) were purchased from the Department of Organic Chemistry, School of Pharmacy, Second Military Medical University (Shanghai China). HNPG is a pale yellow crystalline powder. Its molecular formula is  $C_{18}H_{13}O_7N$  with a molecular weight of 355, and its chemical structure is presented in Figure 1. HNPG and GEN were dissolved in dimethyl sulfoxide (DMSO) into 0.1% (v/v) stock solution until use, and at this concentration there is no effect on cell proliferation. Taxol (TAX) was bought from Molbase Technology Co., Ltd. (catalog number: SJ0033A332183; Wuhan, Hubei, China). DMSO, PBS, and

MTT were obtained from Tiangen Biotech Co., Ltd. (Beijing, China). Giemsa, crystal violet, and hematoxylin and eosin (H&E) stains were all bought from Sangon Biotech Co., Ltd. (Shanghai, China). Matrigel™ was purchased from Shanghai Invitrogen Biological Technology Co., Ltd. (Shanghai, China). Specific antibodies for rabbit anti-β-catenin (Catalog Number: A00183), rabbit anti-C-myc (catalog number: D110006) and rabbit Cyclin D1 (Catalog Number: D151941) were obtained from Sangon Biotech Co., Ltd. (Shanghai, China). Rabbit anti-MMP-2 (catalog number: M00286), rabbit anti-MMP-7 (catalog number: PB0071), rabbit anti-MMP-9 (catalog number: BA2202), rabbit anti-GAPDH antibodies (catalog number: A00227-1) and horseradish peroxidase-conjugated secondary rabbit antibody (catalog number: BA1082) were obtained from Boster Biotech Co., Ltd. (Wuhan, Hubei, China).

### Cell culture

JEC cells were purchased from the cell library of the Chinese Academy of Science (Shanghai, China) and cultured in RPMI-1640 (Thermo Fisher Scientific, Inc., Waltham, MA, USA) that contained 10% fetal bovine serum (FBS; HyClone™, GE Healthcare, Logan, UT, USA) and antibiotic antimycotic solution (100×; Mediatech, Inc., Manassas, VA, USA) at 37°C in a 5% CO<sub>2</sub> humidified incubator. The cells were then divided into 6 groups: the control group (0.1% DMSO), the TAX (Taxol) group, the GEN group, and 3 groups with different concentrations of HNPG (2, 4, and 8 μM).

### The MTT cell proliferation assay

JEC cells were seeded into a 96-well plate (Tiangen Biotech Co., Ltd., Beijing, China) at a density of  $1 \times 10^4$  cells/well and incubated with different concentrations of TAX (0.05, 0.1, 0.2, 0.4, 0.8, 1.6, 3.2, 6.4, and 12.8 μM), GEN (0.5, 1, 2, 4, 8, 16, 32, 64, and 128 μM), and HNPG (0.125, 0.25, 0.5, 1, 2, 4, 8, 16, and 32 μM) for 24 h at 37°C in 5% CO<sub>2</sub>. Subsequently, 20 μl of 5 mg/ml MTT stock solution was added to each well and continued to culture for 6 h at 37°C. A total of 100 μl DMSO was used to stop the reaction, and spectrophotometric absorbance was subsequently measured using a microplate reader (ELX-800; Sangon Biotech Co., Ltd., Shanghai, China) at 570 nm (A570). The values of half maximal inhibitory concentration (IC50) of TAX, GEN, and HNPG were obtained according to the value of spectrophotometric absorbance. We used 0.8 μM TAX, 16 μM GEN, and HNPG (2, 4, and 8 μM) in the subsequent experiments to measure the inhibitive rates for 24, 48, and 72 h. The inhibitive rate (IR) was calculated as follows:  $(1 - \text{average A570 of the experimental group} / \text{average A570 of the control group}) \times 100\%$ . Experiments were performed in triplicate, and the mean value was calculated.

### Flat plate clone formation method

JEC cells were collected and seeded into a 6-well plate (Tiangen Biotech Co., Ltd., Beijing, China) at a density of  $2 \times 10^3$  cells/well and incubated for 24 h at 37°C in 5% CO<sub>2</sub>. Then, 0.1% DMSO, 0.8 μM TAX, 16 μM GEN, and different concentrations of HNPG (2, 4, or 8 μM) were added to each well and cultured for 7 days at 37°C in 5% CO<sub>2</sub> until visible clones formed. Clones containing >50 cells were defined as 1 clone, and were fixed with 95% methanol for 15 min at 20°C and stained with 0.1% Giemsa stain for 15 min at 20°C. The numbers of colonies were computed and the clone formation inhibition rate (%) was calculated as follows:  $1 - (\text{the mean number of HNPG group} / \text{the mean number of control group}) \times 100\%$ . The results were representative of 3 independent experiments [18,19].

### Transwell assay

A pre-cooled 24-well Transwell plate (Tiangen Biotech Co., Ltd., Beijing, China) was covered with 30 μl Matrigel™ at a 1: 3 dilution and incubated at 37°C for 3 h. Then, JEC cells ( $1 \times 10^5$ /well) were cultivated at 37°C for 18 h in the inner chamber and exposed to 100 μl 0.1% FBS/RPMI-1640 with 0.1% DMSO, 0.8 μM TAX, 16 μM GEN, and different concentrations of HNPG (2, 4, or 8 μM), and the outer chamber was filled with 500 μl of 10% FBS/RPMI-1640 to act as a chemoattractant. Subsequently, the invasive cells were fixed with 95% ethanol for 15 min at 20°C, and then stained with 0.5% H&E stain for 15 min at 20°C. JEC cells ( $1 \times 10^5$ /well) were seeded into the inner chamber of 24-well Transwell plate, treated with 100 μl 0.1% FBS/RPMI-1640 containing 0.1% DMSO, 0.8 μM TAX, 16 μM GEN, and different concentrations of HNPG (2, 4, or 8 μM), while the outer chamber contained 500 μl 10% FBS/RPMI-1640, and the Transwell instrument were cultured for 18 h at 37°C. Following this, the metastasized cells were fixed with 4% paraformaldehyde for 15 min at 20°C and subsequently stained with 0.1% crystal violet stain for 15 min at 20°C. The number of invasive cells or metastasized cells was manually counted in 5 randomly selected fields under an inverted microscope (Type: N-STORM 4.0; Nikon instruments co. Ltd., Shanghai, China) with 200 x magnification. Every group had 3 repeat wells and the average value was calculated [3,11].

### Cell cycle analysis

JEC cells were treated with 0.1% DMSO, 0.8 μM TAX, 16 μM GEN, and different concentrations of HNPG (2, 4, or 8 μM) for 48 h, then rinsed with PBS twice, digested with 0.25% trypsin, centrifuged 800 rpm for 5 min at 20°C, and fixed in 70% ethanol at 4°C. Subsequently, the cells were stained with PI (50 mg/ml) solution (Tiangen Biotech Co., Ltd., Beijing, China) at 20°C for 15 min in the dark, and then analyzed using flow cytometry for distribution of cell cycle phase. Excitation and emission

**Table 1.** Primers for quantitative real-time polymerase chain reaction (qRT-PCR).

Name	Primer	Sequence	Size (bp)
β-catenin	Forward	5'-ATGCGGCTGCTGTCTATTC-3'	143
	Reverse	5'-ACCAATGTCCAGTCCGAGAT-3'	
C-myc	Forward	5'-CCTACCCTCTCAACGACAGC-3'	179
	Reverse	5'-TTCCTCCTCAGAGTCTGC-3'	
Cyclin D1	Forward	5'-TTCGTGCGCCTCTGTGCCA-3'	196
	Reverse	5'-GAAGCGTGTGAGCGGTAGTAG-3'	
MMP-2	Forward	5'-TGACATCAAGGGCATTTCAGGAGC-3'	180
	Reverse	5'-GTCCGCCAATGAACGGTCTTG-3'	
MMP-7	Forward	5'-AGGCTCAGGACTATCCTAA-3'	276
	Reverse	5'-CCACTGTAATATGCGGTAAG-3'	
MMP-9	Forward	5'-TGGGCACATCATAACATCAC -3'	158
	Reverse	5'-ATGACAATGCCGCTTCG -3'	
GAPDH	Forward	5'-TACCCACGGCAAGTTCAACG-3'	122
	Reverse	5'-CACCCAGCATCACCCATTG-3'	

wavelengths of 488 nm were selected, experiments were performed in triplicate, and the mean value was calculated.

#### Atomic force microscope (AFM) measurement

We seeded  $1 \times 10^8$  JEC cells in logarithmic phase into a 35-mm cell culture dish, and cultured them in 0.1% DMSO, 0.8  $\mu$ M TAX, 16  $\mu$ M GEN, and different concentrations of HNPG (2, 4, or 8  $\mu$ M) for 24 h, then fixed cells for 6 min at 20°C using 4% paraformaldehyde and rinsed them 2 times with PBS buffer. Then, the changes of morphology were observed and imaged and the Rq and Ra were detected using atomic force microscopy (NanoScope IIIa MultiMode; Veeco Inc., New York, USA). The radius of the microcantilever probe was less than 10 nm, the force elastic coefficient of microcantilever was 5 N/m, and the length and width of the microcantilever were 125  $\mu$ m and 25  $\mu$ m, respectively. The scan ranged from 60 $\times$ 60  $\mu$ m<sup>2</sup> to 5 $\times$ 5  $\mu$ m<sup>2</sup>, and the scanning frequency was 1 Hz. The mechanical measurement of single cells was detected using contact mode in RPMI-1640 medium at 1.63 m/s of moving forward speed and 0.8 Hz of scanning speed. DNP-S of the AFM probe was used to draw the curve of force-distance. The resonant frequency of the probe ranged from 12 kHz to 24 kHz, the force elastic coefficient of the microcantilever was 0.06 N/m, and the length and width of the microcantilever were 205  $\mu$ m and 25  $\mu$ m, respectively. At least 15 cells were selected and more than 1000 curves of force-distance were measured in each group. Young's modulus and adhesion force of Gaussian fitting were analyzed and calculated using Nano Scope analysis software 8.14.

#### Quantitative real-time polymerase chain reaction (qRT-PCR)

The total RNA of JEC cells treated with 0.1% DMSO or different concentrations of HNPG (2, 4, and 8  $\mu$ M) for 24 h was extracted using Trizol (Invitrogen Inc., Carlsbad, California, USA). The RNA purity was detected by ultraviolet spectrophotometer (Product number: UH5300; Yi De Science Instrument Co., Ltd., Guangzhou, China) and the RNA integrity was analyzed using agarose gel electrophoresis. One  $\mu$ g of total RNA was reversely transcribed to cDNA using the Revert Aid™ First-Strand cDNA Synthesis Kit (Fermentas Inc., Shanghai, China) according to the manufacturer's protocol. The qRT-PCR procedure was performed using the SYBR® Premix Ex Taq™ II (Tli RNaseH Plus) system (TaKaRa Inc., Dalian, Liaoning, China) in an Applied Biosystems 7500 fast real-time PCR machine (ABI Inc., Carlsbad, CA, US). The primer sequences are shown in Table 1. The qRT-PCR program was set as initial denaturation at 95°C for 5 min, 40 reaction cycles, with each cycle consisting of a denaturation at 95°C for 15 s, annealing at 60°C for 30 s, and then elongation at 72°C for 30 s. GAPDH mRNA served as the internal control. The value of cycle threshold (CT) was recorded and the mRNA levels of target genes was obtained using the equation of  $2^{-\Delta\Delta CT}$  for each group.

#### Western blotting analysis

JEC cells that were administered 0.1% DMSO or different concentrations of HNPG (2, 4, and 8  $\mu$ M) for 24 h were lysed in 5% lysis buffer (Tiangen Biotech Co., Ltd., Beijing, China). The amount of total protein was determined by BCA kit (Tiangen



Biotech Co., Ltd., Beijing, China). Protein (20  $\mu\text{g}$ ) was separated by 10% SDS-PAGE and transferred to nitrocellulose membranes. Nonspecific binding sites were blocked by incubating the nitrocellulose membrane for 1 h at 37°C with 5% non-fat dried milk in TBST. The membranes were incubated for overnight at 4°C with primary antibodies (rabbit anti- $\beta$ -catenin, rabbit anti-C-myc, rabbit anti-Cyclin D1, rabbit anti-MMP-2, rabbit anti-MMP-7, rabbit anti-MMP-9, and rabbit anti-GAPDH) on a shaker table, and then a horseradish peroxidase-conjugated secondary rabbit antibody was added and shaken for 1 h at 20°C. Bands were visualized using an enhanced chemiluminescence system (Catalog Number: AR1170; Boster Biological Technology Co., Ltd., Wuhan, Hubei, China) and analyzed using Alpha Image 2200 (Version: 1.0; National Institutes of Health, Maryland, USA). Each experiment was repeated 3 times and the mean value was obtained.

### Statistical analysis

SPSS 18.0 software package (SPSS Inc., Chicago, IL, USA) was used for analysis. Data are presented as the mean  $\pm$  standard deviation. The means of multiple groups were compared with one-way analysis of variance (ANOVA),  $P < 0.05$  was considered to indicate a statistically significant difference.

## Results

### HNPG inhibited the proliferation of JEC cells

JEC cells were treated with different concentrations of TAX, GEN, and HNPG respectively ranging from 0.01–12.8  $\mu\text{M}$ , 0.5–128  $\mu\text{M}$ , and 0.125–32  $\mu\text{M}$  for 24 h, and the proliferation of JEC cells was inhibited by TAX, GEN, and HNPG in a dose-dependent manner, and IC50 were 0.78  $\mu\text{M}$ , 16.24  $\mu\text{M}$ , and 3.86  $\mu\text{M}$ , respectively. TAX 0.8  $\mu\text{M}$ , GEN 16  $\mu\text{M}$ , and HNPG (2, 4, and 8  $\mu\text{M}$ ) were used in subsequent experiments to measure the inhibitive rates for 24, 48, and 72 h. The proliferation of JEC cells was markedly inhibited in a dose- and time-dependent manner, the inhibition rate of every HNPG-treated group was significantly different compared with the control group ( $P_{2 \mu\text{M}/0.1\% \text{DMSO}} < 0.05$ ,  $P_{4 \mu\text{M}/0.1\% \text{DMSO}} < 0.05$ ,  $P_{8 \mu\text{M}/0.1\% \text{DMSO}} < 0.05$ ), there was a statistically significant difference among each HNPG-treated group ( $P_{2/4 \mu\text{M}} < 0.05$ ,  $P_{2/8 \mu\text{M}} < 0.05$ ,  $P_{4/8 \mu\text{M}} < 0.05$ ), and there were no significant differences among HNPG 4  $\mu\text{M}$ , GEN 16  $\mu\text{M}$ , and TAX 0.8  $\mu\text{M}$  ( $P_{\text{HNPG of } 4 \mu\text{M}/\text{GEN of } 16 \mu\text{M}} > 0.05$ ,  $P_{\text{HNPG of } 4 \mu\text{M}/\text{TAX of } 0.8 \mu\text{M}} > 0.05$ ,  $P_{\text{TAX of } 0.8 \mu\text{M}/\text{GEN of } 16 \mu\text{M}} > 0.05$ ) (Figure 2A–2D).

### HNPG suppressed the clone formation of JEC cells

JEC cells were incubated at 37°C with 0.1% DMSO, TAX 0.8  $\mu\text{M}$ , GEN 16  $\mu\text{M}$ , and different concentrations of HNPG (2, 4, or 8  $\mu\text{M}$ ) for 7 days. The rate of clone formation was dramatically

reduced and the numbers of cells inside the clones were significantly decreased. The inhibition rate of clone formation was significantly increased in a dose-dependent manner and every HNPG-treated group demonstrated a marked difference compared with the control group ( $P_{2 \mu\text{M}/0.1\% \text{DMSO}} < 0.05$ ,  $P_{4 \mu\text{M}/0.1\% \text{DMSO}} < 0.05$ ,  $P_{8 \mu\text{M}/0.1\% \text{DMSO}} < 0.05$ ). In addition, there was a significant difference among each HNPG-treated group ( $P_{2/4 \mu\text{M}} < 0.05$ ,  $P_{2/8 \mu\text{M}} < 0.05$ ,  $P_{4/8 \mu\text{M}} < 0.05$ ) but there was no significant difference among TAX 0.8  $\mu\text{M}$ , GEN 16  $\mu\text{M}$ , and HNPG 4  $\mu\text{M}$  ( $P_{\text{HNPG of } 4 \mu\text{M}/\text{TAX of } 0.8 \mu\text{M}} > 0.05$ ,  $P_{\text{HNPG of } 4 \mu\text{M}/\text{GEN of } 16 \mu\text{M}} > 0.05$ ,  $P_{\text{GEN of } 16 \mu\text{M}/\text{TAX of } 0.8 \mu\text{M}} > 0.05$ ) (Figure 2E, 2F).

### HNPG inhibited the invasion ability of JEC cells

JEC cells were cultured with 0.1% DMSO, TAX 0.8  $\mu\text{M}$ , GEN 16  $\mu\text{M}$ , and different concentrations of HNPG (2, 4, or 8  $\mu\text{M}$ ) for 18 h, and the invasive ability was markedly decreased in a dose-dependent manner. The results demonstrated that the average cell numbers of 0.1% DMSO, TAX 0.8  $\mu\text{M}$ , GEN 16  $\mu\text{M}$ , and different concentrations of HNPG (2, 4, or 8  $\mu\text{M}$ ) groups invading through the Matrigel were 65.42 $\pm$ 5.64, 24.38 $\pm$ 3.16, 26.74 $\pm$ 3.26, 40.86 $\pm$ 4.71, 22.54 $\pm$ 3.26, and 12.37 $\pm$ 1.61, respectively. There was a significant difference between each HNPG-treated group and the control ( $P_{2 \mu\text{M}/0.1\% \text{DMSO}} < 0.05$ ,  $P_{4 \mu\text{M}/0.1\% \text{DMSO}} < 0.05$ ,  $P_{8 \mu\text{M}/0.1\% \text{DMSO}} < 0.05$ ), and there was a significant difference among each HNPG-treated group ( $P_{2/4 \mu\text{M}} < 0.05$ ,  $P_{2/8 \mu\text{M}} < 0.05$ ,  $P_{4/8 \mu\text{M}} < 0.05$ ), but there was no significant difference among TAX 0.8  $\mu\text{M}$ , GEN 16  $\mu\text{M}$ , and HNPG 4  $\mu\text{M}$  ( $P_{\text{HNPG of } 4 \mu\text{M}/\text{TAX of } 0.8 \mu\text{M}} > 0.05$ ,  $P_{\text{HNPG of } 4 \mu\text{M}/\text{GEN of } 16 \mu\text{M}} > 0.05$ ,  $P_{\text{GEN of } 16 \mu\text{M}/\text{TAX of } 0.8 \mu\text{M}} > 0.05$ ) (Figure 3A, 3B).

### HNPG suppressed the metastasis ability of JEC cells

JEC cells were cultivated with 0.1% DMSO, TAX 0.8  $\mu\text{M}$ , GEN 16  $\mu\text{M}$ , and different concentrations of HNPG (2, 4, or 8  $\mu\text{M}$ ) for 18 h, and the metastasizing ability of JEC cells was significantly decreased in a concentration-dependent manner. The results demonstrated that the average cell numbers of 0.1% DMSO, TAX 0.8  $\mu\text{M}$ , GEN 16  $\mu\text{M}$ , and different doses of HNPG (2, 4, or 8  $\mu\text{M}$ ) groups that metastasized through polycarbonate membrane were 88.36 $\pm$ 7.42, 28.45 $\pm$ 3.82, 24.15 $\pm$ 3.21, 44.76 $\pm$ 4.18, 28.72 $\pm$ 3.18, and 13.24 $\pm$ 1.63, respectively. There was a significant difference among every HNPG-treated group. There was a significant difference between each HNPG-treated group and the control ( $P_{2 \mu\text{M}/0.1\% \text{DMSO}} < 0.05$ ,  $P_{4 \mu\text{M}/0.1\% \text{DMSO}} < 0.05$ ,  $P_{8 \mu\text{M}/0.1\% \text{DMSO}} < 0.05$ ), and there was a significant difference among each HNPG-treated group ( $P_{2/4 \mu\text{M}} < 0.05$ ,  $P_{2/8 \mu\text{M}} < 0.05$ ,  $P_{4/8 \mu\text{M}} < 0.05$ ), but there was no significant difference among TAX 0.8  $\mu\text{M}$ , GEN 16  $\mu\text{M}$ , and HNPG 4  $\mu\text{M}$  ( $P_{\text{HNPG of } 4 \mu\text{M}/\text{TAX of } 0.8 \mu\text{M}} > 0.05$ ,  $P_{\text{HNPG of } 4 \mu\text{M}/\text{GEN of } 16 \mu\text{M}} > 0.05$ ,  $P_{\text{GEN of } 16 \mu\text{M}/\text{TAX of } 0.8 \mu\text{M}} > 0.05$ ) (Figure 3C, 3D).

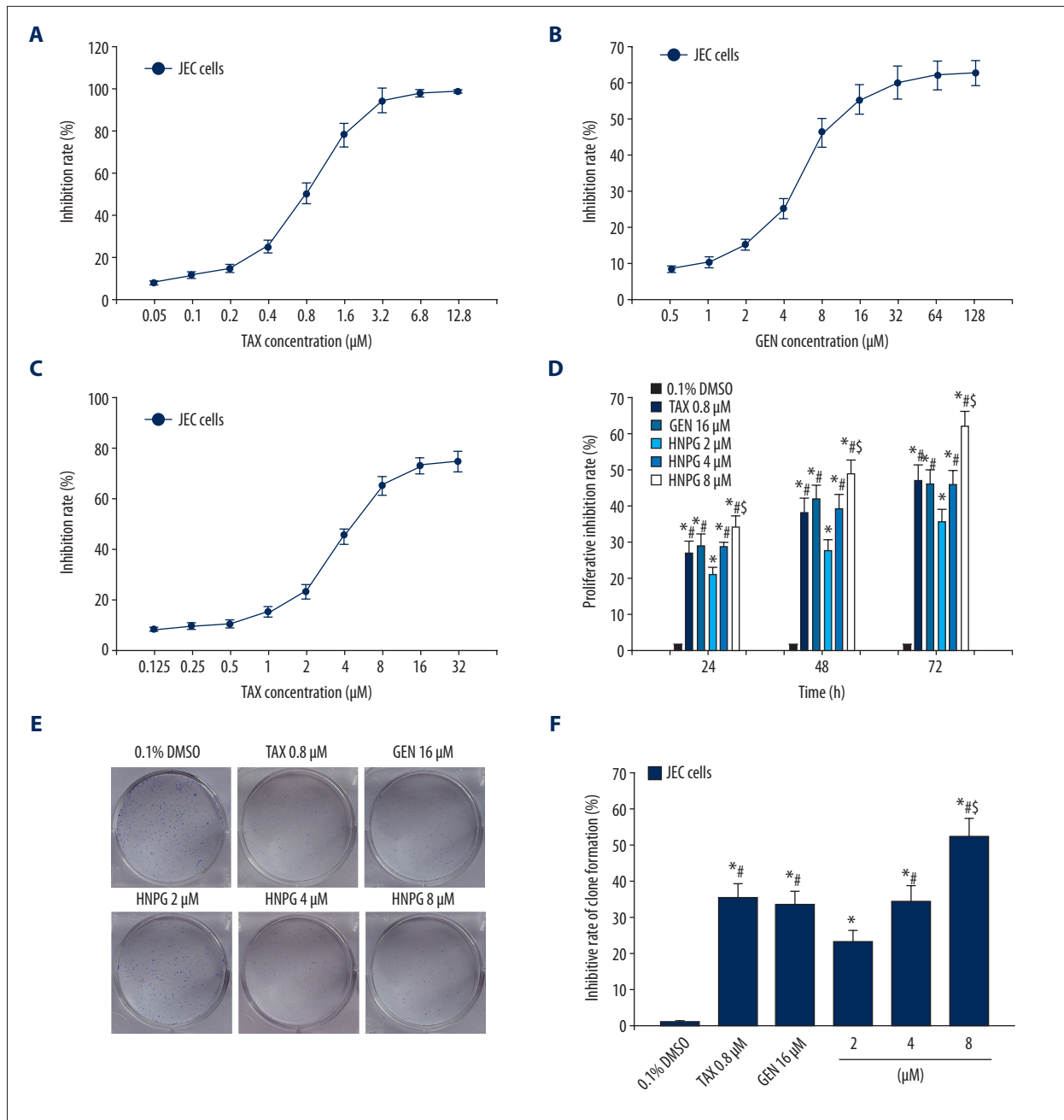


**Figure 2.** Effects of HNPG on the inhibition of cell viability in JEC cells. (A) Graph indicating the rate of proliferative inhibition of TAX ranging from 0.05–12.8 μM for 24 h. (B) Diagram showing the rate of proliferation inhibition of GEN ranging from 0.5–128 μM for 24 h. (C) Graph exhibiting the rate of proliferation inhibition of HNPG ranging from 0.125–32 μM for 24 h. (D) Histograms demonstrating the proliferative inhibition rate of 0.1% DMSO, TAX 0.8 μM, GEN 16 μM, and different concentrations of HNPG (2, 4, or 8 μM) for 24, 48 and 72 h. (E) Images indicating the clone formation of JEC cells exposed to 0.1% DMSO, TAX 0.8 μM, GEN 16 μM, and different concentrations of HNPG (2, 4, or 8 μM) for 7 days stained with Giemsa stain. (F) Histogram demonstrating the inhibition rate of clone formation of JEC cells exposed to 0.1% DMSO, TAX 0.8 μM, GEN 16 μM, and different concentrations of HNPG (2, 4, or 8 μM) for 7 days. The data are presented as the mean ± standard deviation from 3 independent experiments. \* P<0.05 vs. 0.1% DMSO group, # P<0.05 vs. 2 μM HNPG group, \$ P<0.05 vs. 4 μM HNPG, or 0.8 μM TAX, or 16 μM GEN.

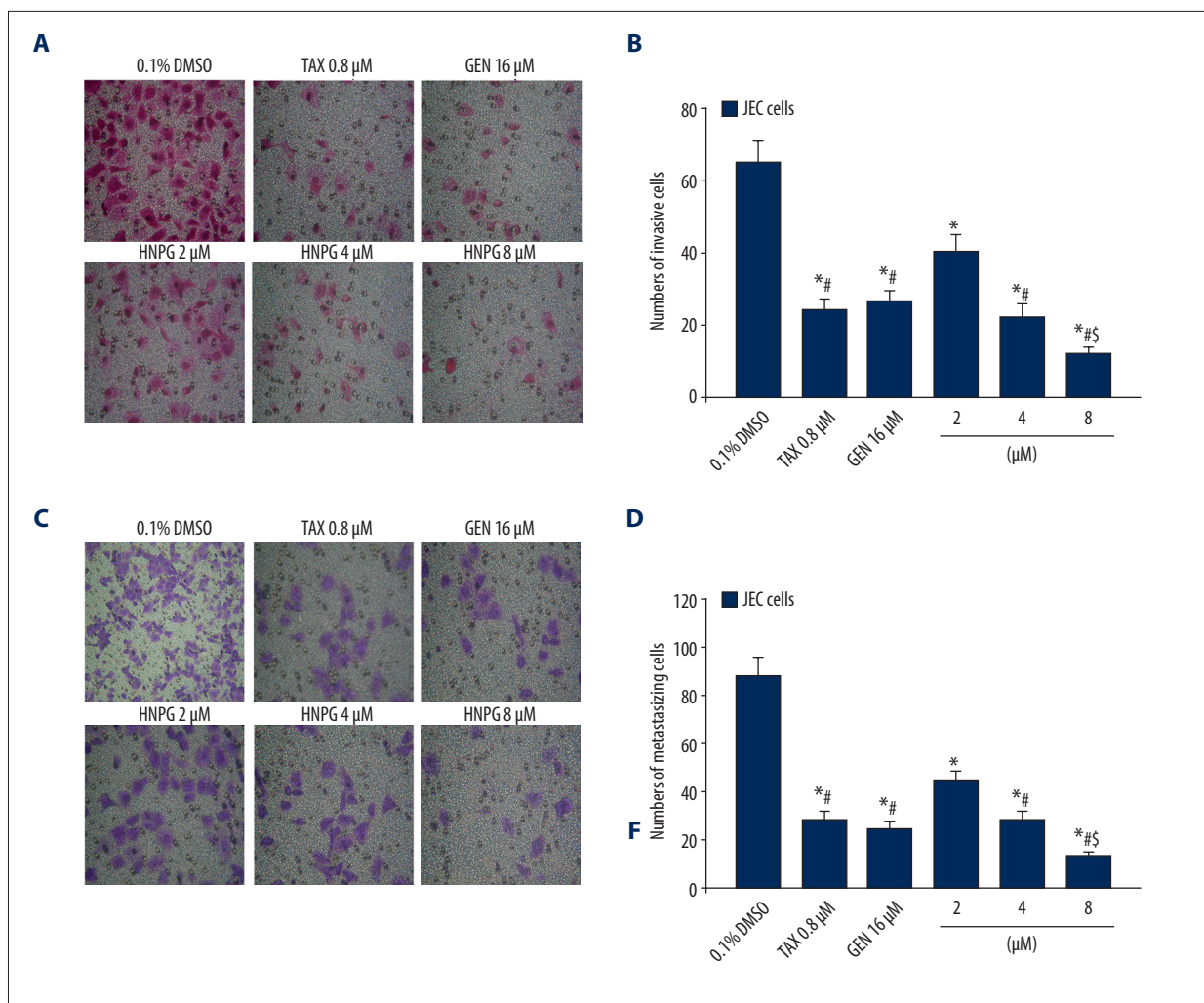


**Figure 3.** Effects of HNPG on the invasive and metastasizing capabilities of JEC cells treated with 0.1% DMSO, TAX 0.8 μM, GEN 16 μM, and different concentrations of HNPG (2, 4, or 8 μM) for 18 h. (A) Images demonstrating JEC cells in a Matrigel assay and stained with H&E stain (magnification, 200×). (B) Histogram exhibiting the numbers of invasive cells via a Matrigel assay. (C) Images indicating JEC cells on a polycarbonate membrane stained with crystal violet stain (magnification, 200×). (D) Histogram showing the cell numbers of metastasis via a polycarbonate membrane. The data are presented as the mean ± standard deviation from 3 independent experiments. \* P<0.05 vs. 0.1% DMSO group, # P<0.05 vs. 2 μM HNPG group, \$ P<0.05 vs. 4 μM HNPG, or 0.8 μM TAX, or 16 μM GEN.

**HNPG induced the accumulation of G1 phase of JEC cells**

JEC cells were exposed to 0.1% DMSO, TAX 0.8 μM, GEN 16 μM, and different concentrations of HNPG (2, 4, or 8 μM) for 48 h, and G1 phase of JEC cells was significantly accumulated. The results indicated that HNPG markedly blocked JEC cells in G1 phase in a dose-dependent manner, the G1 phase of 0.1% DMSO, TAX 0.8 μM, GEN 16 μM, and different concentrations of HNPG (2, 4, or 8 μM) groups were 48.71±2.12%, 72.22±4.15%, 70.76±5.52%, 63.87±4.56%, 72.05±5.21%, and 93.25±6.54%, respectively. Every HNPG-treated group was significantly different from the control group ( $P_{2 \mu\text{M}/0.1\% \text{DMSO}} < 0.05$ ,  $P_{4 \mu\text{M}/0.1\% \text{DMSO}} < 0.05$ ,  $P_{8 \mu\text{M}/0.1\% \text{DMSO}} < 0.05$ ), and there were

significant differences among each HNPG-treated group ( $P_{2/4 \mu\text{M}} < 0.05$ ,  $P_{2/8 \mu\text{M}} < 0.05$ ,  $P_{4/8 \mu\text{M}} < 0.05$ ), but there were no significant differences among TAX 0.8 μM, GEN 16 μM, and HNPG 4 μM ( $P_{\text{TAX of } 0.8 \mu\text{M}/\text{HNPG of } 4 \mu\text{M}} > 0.05$ ,  $P_{\text{GEN of } 16 \mu\text{M}/\text{HNPG of } 4 \mu\text{M}} > 0.05$ ,  $P_{\text{GEN of } 16 \mu\text{M}/\text{TAX of } 0.8 \mu\text{M}} > 0.05$ ) (Figure 4A, 4B).

**HNPG changed the morphological features of JEC cells**

The morphology of cells of 0.1% DMSO group was long fusiform, the filamentous pseudopod was distributed around the cell body, and the surface of the cell membrane was relatively flat and covered with granules 60×60 μm<sup>2</sup> of scan range of AFM (Figure 5A). The surface of the cell membrane showed

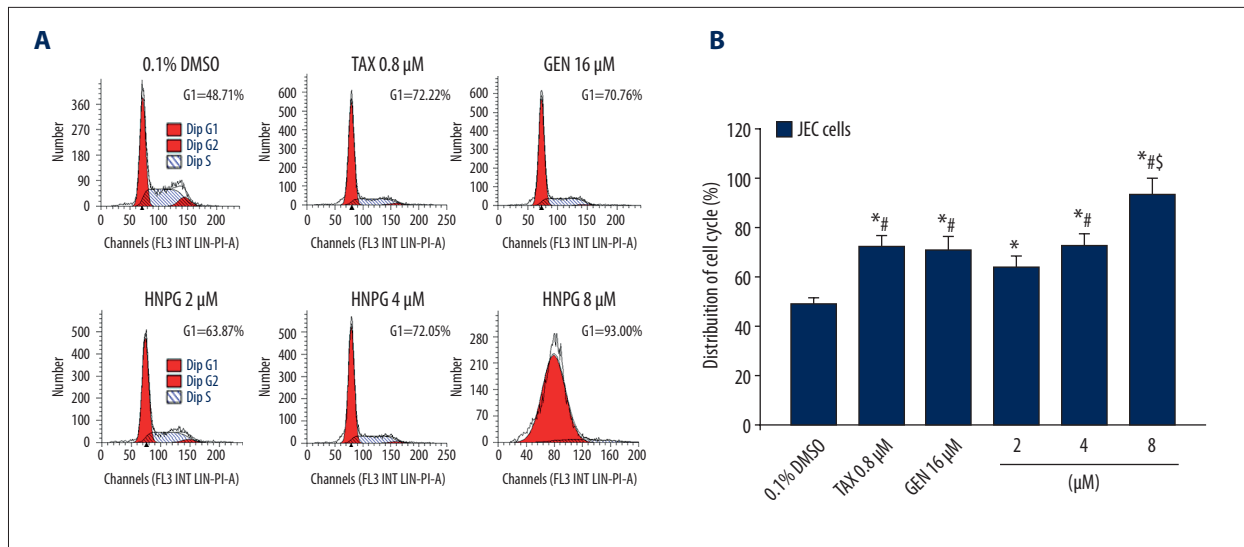


**Figure 4.** Effects of HNPG on the accumulation in G1 phase in JEC cells cultured with 0.1% DMSO, TAX of 0.8 μM, GEN 16 μM, and different concentrations of HNPG (2, 4, or 8 μM) for 48 h. (A) Diagrams exhibiting the distribution of cell cycle percentage of JEC cells stained with PI. (B) Histogram demonstrating the distribution of cell cycle percentage rate. The data are presented as the mean ± standard deviation from 3 independent experiments. \* P<0.05 vs. 0.1% DMSO group, # P<0.05 vs. 2 μM HNPG group, § P<0.05 vs. 4 μM HNPG, or 0.8 μM TAX, or 16 μM GEN.

the shape of a flannelette blanket with small homogeneous bulges. The arrangement of bulges was moderate in 5×5 μm<sup>2</sup> of scanning range, which is characterized by normal malignant tumor cells (Figure 5A). When cells were treated by 0.1% DMSO, TAX 0.8 μM, GEN 16 μM, and different concentrations of HNPG (2, 4, or 8 μM) after 24 h, the morphology of JEC cells obviously changed in a concentration-dependent manner; the cell body retracted, the filamentary pseudopod disappeared, the surface of the cell membrane appeared to have holes of unequal size, the nucleus collapsed, the height of the nucleus decreased, and the ultrastructure showed there were irregular bumps around the hole of the cell membrane, which indicated that the cells were obviously damaged. The degree of damage caused by HNPG 40 μM was approximately similar to that of TAX 0.8 μM or GEN 16 μM (Figure 5A).

#### HNPG decreased the root-mean-square roughness (Rq) and the average roughness (Ra) of JEC cells

The present study found that the root-mean-square roughness (Rq) of 0.1% DMSO, TAX 0.8 μM, GEN 16 μM, and different concentrations of HNPG (2, 4, or 8 μM) was 113.0±7.51 nm, 49.57±5.40 nm, 48.33±3.72 nm, 57.42±3.78 nm, 46.87±3.67 nm, and 35.77±4.24 nm, respectively. In addition, the average roughness (Ra) of 0.1% DMSO, TAX 0.8 μM, GEN 16 μM, and different concentrations of HNPG (2, 4, or 8 μM) was 83.97±5.83 nm, 35.20±4.50 nm, 37.97±3.13 nm, 56.93±4.49 nm, 35.73±4.72 nm, and 26.43±2.33 nm, respectively. The Rq and Ra of every HNPG-treated group possessed statistical difference compared with control group ( $P_{2\mu\text{M}/0.1\% \text{DMSO}} < 0.05$ ,

$P_{4\mu\text{M}/0.1\% \text{DMSO}} < 0.05$ ,  $P_{8\mu\text{M}/0.1\% \text{DMSO}} < 0.05$ ), and there were significant differences among the Rq and Ra of each HNPG-treated group ( $P_{2/4\mu\text{M}} < 0.05$ ,  $P_{2/8\mu\text{M}} < 0.05$ ,  $P_{4/8\mu\text{M}} < 0.05$ ), but there were no significant differences among the Rq and Ra of TAX 0.8 μM, GEN 16 μM, and HNPG 4 μM ( $P_{\text{TAX of } 0.8\mu\text{M}/\text{HNPG of } 4\mu\text{M}} > 0.05$ ,  $P_{\text{GEN of } 16\mu\text{M}/\text{HNPG of } 4\mu\text{M}} > 0.05$ ,  $P_{\text{GEN of } 16\mu\text{M}/\text{TAX of } 0.8\mu\text{M}} > 0.05$ ) (Figure 5C, 5D).

#### HNPG increased Young's modulus and adhesion force of Gaussian fitting of JEC cells

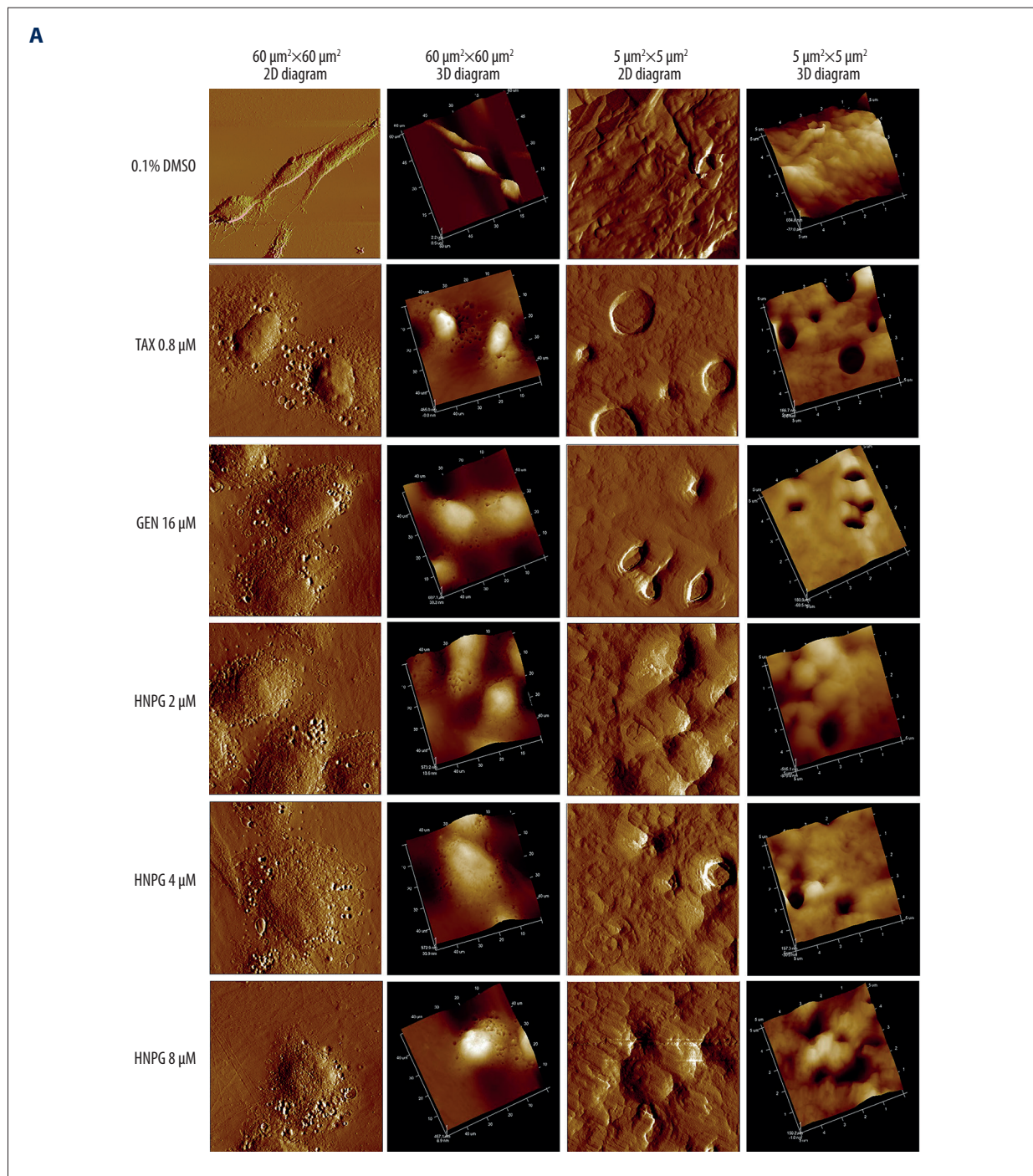
The mechanical detection of individual living cell was measured using AFM indentation technique, and the value of Young's modulus of Gaussian fitting was 7.53±0.62 kPa, 17.72±1.57 kPa, 18.39±1.58 kPa, 12.53±1.14 kPa, 18.18±1.73 kPa, and 20.46±1.16 kPa, respectively. The nonspecific forces between the cell surface and the probe were detected using AFM indentation technique, and the adhesion force of Gaussian fitting between the cell surface and the probe was 53.23±4.01 pN, 69.36±5.36 pN, 69.10±5.03 pN, 62.62±7.97 pN, 73.49±5.23 pN, and 80.19±6.13 pN, respectively. Young's modulus and adhesion force of Gaussian fitting of every HNPG-treated group were significantly different compared with the control group ( $P_{2\mu\text{M}/0.1\% \text{DMSO}} < 0.05$ ,  $P_{4\mu\text{M}/0.1\% \text{DMSO}} < 0.05$ ,  $P_{8\mu\text{M}/0.1\% \text{DMSO}} < 0.05$ ), and there were significant differences among Young's modulus and adhesion force of Gaussian fitting of each HNPG-treated group ( $P_{2/4\mu\text{M}} < 0.05$ ,  $P_{2/8\mu\text{M}} < 0.05$ ,  $P_{4/8\mu\text{M}} < 0.05$ ), but there were no significant differences among Young's modulus and adhesion force of Gaussian fitting of TAX of 0.8 μM, GEN 16 μM, and HNPG 4 μM ( $P_{\text{TAX of } 0.8\mu\text{M}/\text{HNPG of } 4\mu\text{M}} > 0.05$ ,  $P_{\text{GEN of } 16\mu\text{M}/\text{HNPG of } 4\mu\text{M}} < 0.05$ ,  $P_{\text{GEN of } 16\mu\text{M}/\text{TAX of } 0.8\mu\text{M}} < 0.05$ ) (Figure 6A–6D).



**HNPG regulated mRNA of wnt/ $\beta$ -catenin signal pathway in JEC cells**

JEC cells were administered to 0.1% DMSO and different concentrations of HNPG (2, 4, or 8  $\mu$ M) for 24 h, and the average value of mRNA of  $\beta$ -catenin, C-Myc, Cyclin D1, MMP-2, MMP-7, and MMP-9 were analyzed. The expressive mRNA level of  $\beta$ -catenin, C-Myc, Cyclin D1, MMP-2, MMP-7, and MMP-9 exhibited

a decreasing dose-dependent trend. Every HNPG-treated group exhibited a significant difference compared with the control group ( $P_{2 \mu\text{M}/0.1\% \text{DMSO}} < 0.05$ ,  $P_{4 \mu\text{M}/0.1\% \text{DMSO}} < 0.05$ ,  $P_{8 \mu\text{M}/0.1\% \text{DMSO}} < 0.05$ ) in  $\beta$ -catenin, C-Myc, Cyclin D1, MMP-2, MMP-7, and MMP-9 mRNA expression levels. There were significant differences among every HNPG-treated group in  $\beta$ -catenin, C-Myc, Cyclin D1, MMP-2, and MM-7 and MMP-9 mRNA expression levels ( $P_{2/4 \mu\text{M}} < 0.05$ ,  $P_{2/8 \mu\text{M}} < 0.05$ ,  $P_{4/8 \mu\text{M}} < 0.05$ ) (Figure 7A, 7B).



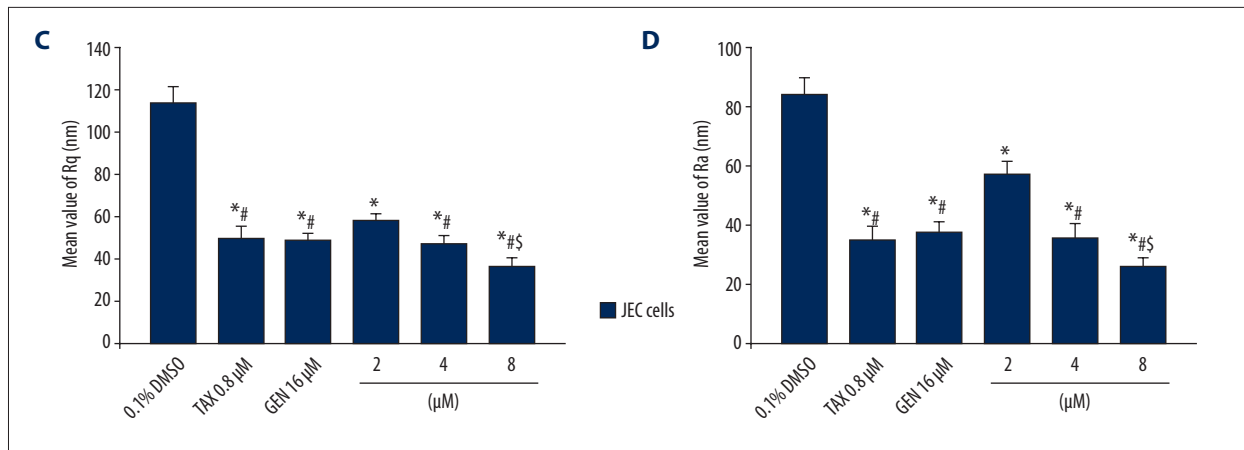


**Figure 5.** The changes of morphological features and the detection of biological force trait using atomic mechanics microscopy (AFM) in JEC cells incubated with 0.1% DMSO, TAX 0.8 μM, GEN 16 μM, and different concentrations of HNPG (2, 4, or 8 μM) for 24 h. (A) Images exhibiting the morphological characteristics of 2- or 3-dimensional diagram of JEC cells in 60×60 μm<sup>2</sup> or 5×5 μm<sup>2</sup> of scan range. (B) Histogram exhibiting the changes of root-mean-square roughness (Rq) of JEC cells. (C) Histogram demonstrating the changes of average roughness (Ra) of JEC cells. The data are indicated as the mean ± standard deviation from 3 independent experiments. \* P<0.05 vs. 0.1% DMSO group, # P<0.05 vs. 2 μM HNPG group, \$ P<0.05 vs. 4 μM HNPG, or 0.8 μM TAX, or 16 μM GEN.

### HNPG regulated protein of wnt/β-catenin signal pathway of JEC cells

JEC cells were exposed to 0.1% DMSO and different concentrations of HNPG (2, 4, or 8 μM) for 24 h, and the average relative density of β-catenin, C-Myc, Cyclin D1, MMP-2, MMP-7, and MMP-9 were analyzed. The expression level of β-catenin, C-Myc, Cyclin D1, MMP-2, MMP-7, and MMP-9 protein exhibited a decreasing concentration-dependent trend. All HNPG-treated groups demonstrated a significant difference compared with the control group ( $P_{2 \mu\text{M}/0.1\% \text{DMSO}} < 0.05$ ,  $P_{4 \mu\text{M}/0.1\% \text{DMSO}} < 0.05$ ,  $P_{8 \mu\text{M}/0.1\% \text{DMSO}} < 0.05$ ) in β-catenin, C-Myc, Cyclin D1, MMP-2, MMP-7, and MMP-9 protein expression levels. There were significant differences among every HNPG-treated group in β-catenin, C-Myc, Cyclin D1, MMP-2, and MMP-9 protein expression levels ( $P_{2/4 \mu\text{M}} < 0.05$ ,  $P_{2/8 \mu\text{M}} < 0.05$ ,  $P_{4/8 \mu\text{M}} < 0.05$ ). There were significant differences between the 2 or 4 μM HNPG-treated group and the 8 μM HNPG-treated groups in MMP-7 protein expression ( $P_{2/8 \mu\text{M}} < 0.05$  or  $P_{4/8 \mu\text{M}} < 0.05$ ), but there were no differences between the 2 and 4 μM HNPG-treated groups in MMP-7 protein expression ( $P_{2/4 \mu\text{M}} > 0.05$ ) (Figure 7C–7E).

### Discussion

Invasion and metastasis are basic characteristics of malignant tumors. Malignant carcinomas not only germinate in the primary site via infiltrating and damaging adjacent organs and tissues, but also metastasize to other areas to proliferate and grow and cause new damage, so the capacities of invasion and metastasis directly reflect the malignant degree of tumors. The

capacity of inhibiting invasion and metastasis are also becoming one of the normal indices used to evaluate pharmacological activity [20,21]. It was reported that GEN exerts a molecular biological function via competitively combining with ER with estrone (E1) and estradiol (E2) in the cells that expressed ER, and GEN could affect biological characters via other cellular signal pathways, such as accumulating tumor cells in G2/M phase, inhibiting proliferation, inducing apoptosis, regulating angiopoiesis, anti-oxygenation, and adjusting the expression of oncogenes in breast cancer [22,23]. GEN has no cell toxic effects on normal cells, but it possesses significant cytotoxicity for many tumor cells [24]. As a new derivative of GEN, previous studies had demonstrated that HNPG could inhibit proliferation in gastric and breast cancer cells *in vitro* [8,9], but the therapeutic effect of HNPG has not been investigated and its molecular mechanism has not yet been elucidated. In the present study, the data indicated that HNPG could suppress proliferation, clone formation, invasion, and metastasis, and accumulated G1 phase in human endometrial cancer JEC cells *in vitro*. These experimental results suggest HNPG may be an excellent novel candidate for therapy in human endometrial cancer.

Cells proliferate via cell cycle, with 1 cell dividing into 2 cells, and must go through first gap phase (G1), synthetic phase (S), second gap phase (G2), and mitotic phase (M) in sequence; any cell phases that encounter obstacles will result in cell proliferation stasis and even apoptosis or necrosis, which will affect the function of cell viability such as proliferation, colony formation, invasion, and metastasis [25]. When external factors and internal factors cause cell cycle damage, the permeability

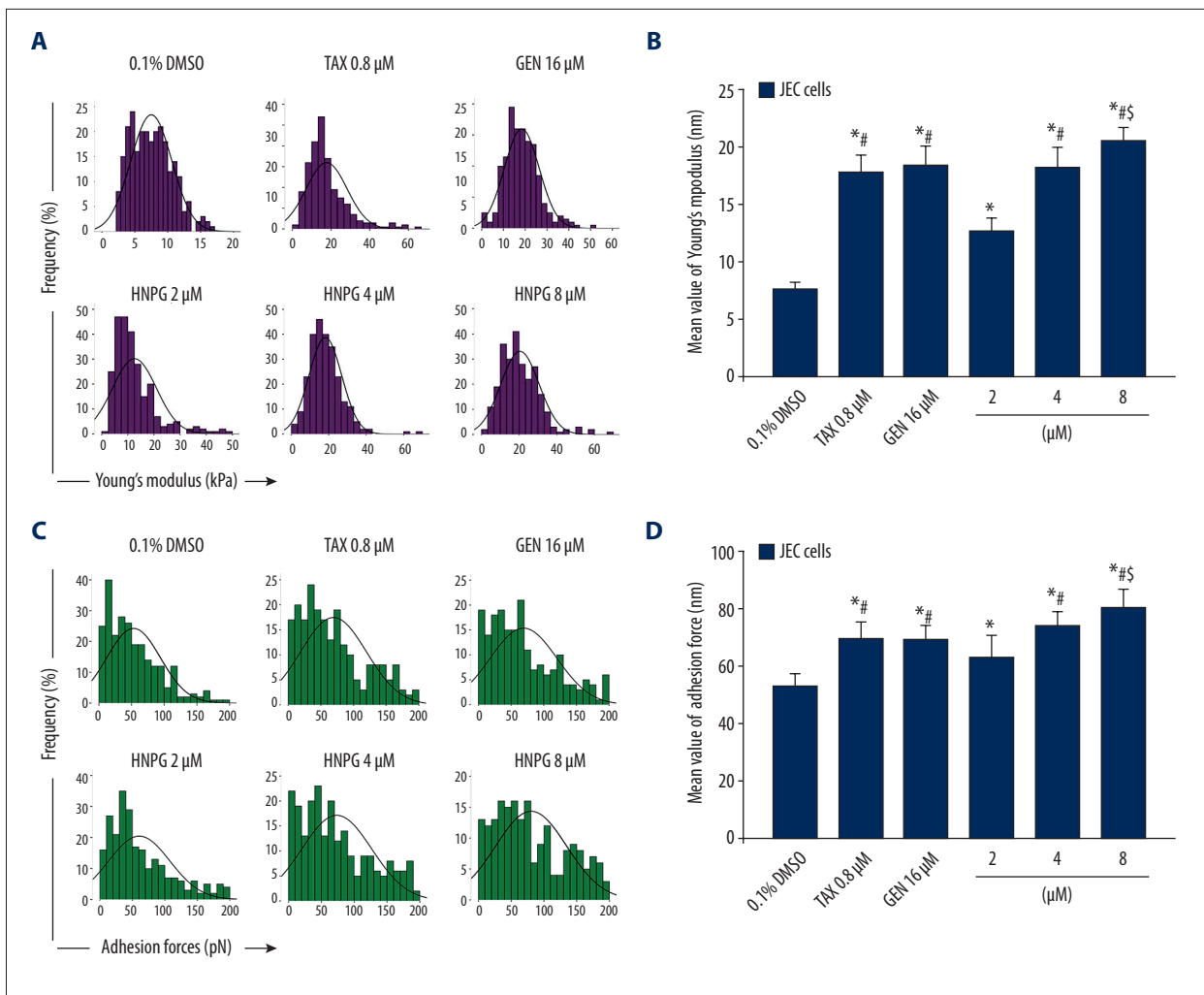


**Figure 6.** The biological force trait using atomic mechanics microscopy (AFM) in JEC cells incubated with 0.1% DMSO, TAX 0.8 μM, GEN 16 μM, and different concentrations of HNPG (2, 4, or 8 μM) for 24 h. (A) Diagrams demonstrating the changes of Young's Modulus of Gaussian fitting of JEC cells. (B) Histograms indicating the mean value of Young's Modulus of JEC cells. (C) Diagrams showing the changes of the adhesive force of Gaussian fitting of JEC cells. (D) Histograms exhibiting the mean value of the adhesive force of JEC cells. The data are indicated as the mean ± standard deviation from 3 independent experiments. \* P<0.05 vs. 0.1% DMSO group, # P<0.05 vs. 2 μM HNPG group, \$ P<0.05 vs. 4 μM HNPG, or 0.8 μM TAX, or 16 μM GEN.

of the cell membrane will be increased, which causes propidium iodide (PI) to enter the cytoplasm through the cell membrane and combine with DNA in the nucleus [26]. The content of DNA in different cell phases is different: the feature of DNA in G1 phase is characterized in diploid cells, the trait of DNA in G2 phase is represented in tetraploid cells, while the characteristics of DNA in S phase is between diploid cells and tetraploid cells. Different cell phases are distinguished via detecting the intensity of PI fluorescence combining with DNA by flow cytometry [27]. In the results of the present study, the numbers of JEC cells in G1 phase were markedly enhanced in a dose-dependent manner following HNPG treatment for 48 h, suggesting that the HNPG-mediated inhibition of proliferation,

clone formation, invasion, and metastasis of JEC cells might occur via the accumulation in G1 phase.

It is well known that cell proliferation has to go through check points regulated by cyclin, cyclin-dependent kinase (CDK), and cyclin-dependent kinase inhibitor (CKI) [27]. The check point of G1/S is one of the most important check points in the progression of the cell cycle. When the check point of G1/S receives the signal information of DNA damage, it will interrupt the progression of the cell cycle and block cells in G1 phase [27]. Cyclin D1 is the most important regulatory factor in G1/S; it can combine with CDK2, CDK4, and CDK6, and promote cells to go through G1/S check point and enter S phase [27].

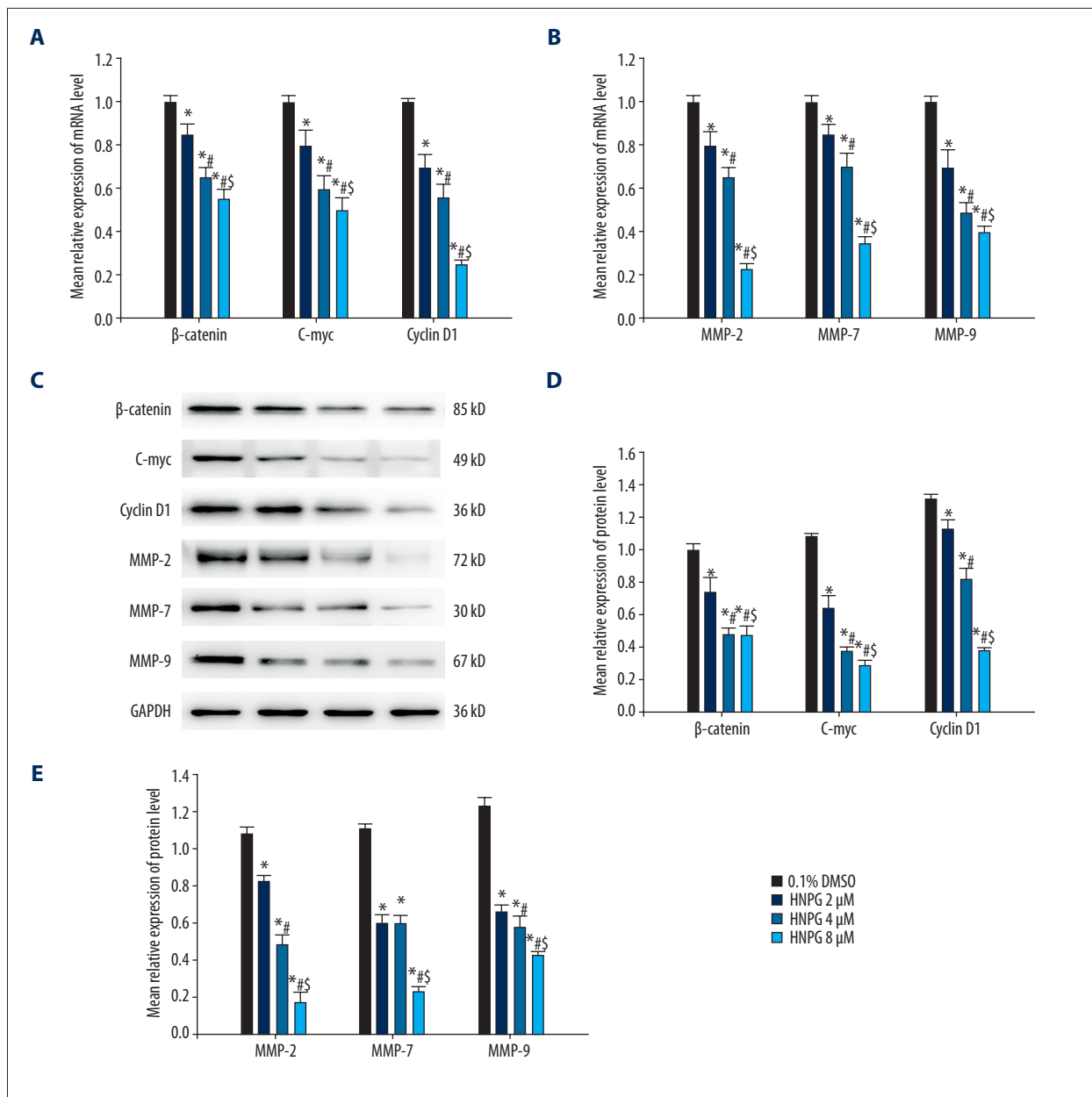


**Figure 7.** The changes of gene expression of JEC cells incubated with 0.1% DMSO, and different concentrations of HNPG (2, 4, or 8 μM) for 24 h. (A) Histogram demonstrating the average relative expression of mRNA level of β-catenin, C-Myc, and Cyclin D1. (B) Histogram indicating the mean relative expression of mRNA of MMP-2, MMP-7, and MMP-9. (C) Electrophoretograms showing the expression of protein level of β-catenin, C-Myc, Cyclin D1, MMP-2, MMP-7, and MMP-9. (D) Histogram demonstrating the average relative expression of protein level of β-catenin, C-Myc, and Cyclin D1. (E) Histogram exhibiting the mean relative expression of protein level of MMP-2, MMP-7, and MMP-9. The data were shown as the mean ± standard deviation from 3 independent experiments. \* P<0.05 vs. 0.1% DMSO group, # P<0.05 vs. 2 μM HNPG group, \$ P<0.05 vs. 4 μM HNPG, or 0.8 μM TAX, or 16 μM GEN.

When the amount of Cyclin D1 increases in cells, the proliferative speed increases and causes tumors and other diseases. Conversely, if the amount of Cyclin D1 decreases, cells will accumulate in G1 phase, which will result in cell function decline, including invasion and metastasis [27,28]. C-Myc can

promote cell proliferation via regulating several genes related to proliferation including Cyclin D1 [28]. C-Myc and Cyclin D1 are closely related to tumorigenesis, invasion, and metastasis [27,28]. In the present study, C-Myc and Cyclin D1 of JEC cells incubated with different concentrations of HNPG were



notably downregulated in a dose-dependent manner, accompanied by the accumulation of G1 phase, which suggests that the accumulation of G1 phase might be related to the downregulation of C-Myc and Cyclin D1.

Degradation of extracellular matrix (ECM) is an important element of invasion and metastasis of malignant tumors, and matrix metalloproteinases (MMPs) are a group of proteolytic enzymes closely related to various pathological processes, especially tumor invasion and metastasis [29,30]. MMP-7, MMP-2, and MMP-9 are important members of the MMP family that can degrade extracellular matrix and basement membrane components. MMP-7, MMP-2, and MMP-9 are upregulated in tumor tissues, regulating tumor cell proliferation and metastasis through degradation of ECM [29,30]. MMP-2 and MMP-9 are type IV collagen enzymes that mainly degrade type IV collagen and laminin [29]. MMP-7 is a special type of MMP with strong degrading activity of ECM and possesses a wide range of biological substrates including type IV collagen, laminin, polysaccharide, type I gelatin, and soluble elastin [30]. In our research, we found HNPG inhibited invasion and metastasis of JEC cells accompanied by MMP-2, MMP-7, and MMP-9 downregulation in a dose-dependent manner, suggesting that MMP-2, MMP-7, and MMP-9 are involved in the effects of HNPG in inhibiting invasion and metastasis.

Adhesion force decreased among cells and amoeba movement depending on pseudopod are the premise conditions of invasion and metastasis in malignant cancer cells [31]. Cells secrete certain adhesive proteins that fasten cells together and prevent cells from metastasizing to other sites [31]. The force produced by those adhesive proteins can be measured using AFM; the adhesive force of malignant cancer tissue is lower than normal tissue, so measuring the adhesive force between cells can reflect the metastasizing capacities of tumor cells [32]. The plasticity or elasticity of cells is the necessary condition of cell migration and Young's modulus is often used to detect the plasticity or elasticity of cells in bioengineering [33]. In the present study, we found JEC cells treated with different concentrations of HNPG became oval, pseudopods disappeared, and the surface roughness (Rq and Ra) decreased, while adhesion force and Young's modulus of Gaussian fitting increased, which were in conjunction with the inhibition of invasion and metastasis. Our research suggests that the inhibition effects of HNPG on invasion and metastasis are related to the alteration of morphology, the decrease of Rq and Ra, and the increase of Young's modulus and adhesive force.

The wnt/ $\beta$ -catenin signal pathway is involved in invasion and metastasis of many cancers and plays a very important role in tumor chemotherapy, including therapy for endometrial cancer [33,34].  $\beta$ -catenin occupies the core position in the wnt/ $\beta$ -catenin signal pathway. When the amount of  $\beta$ -catenin increases in cytoplasm,  $\beta$ -catenin will enter nucleus, which triggers a series of biological reactions, promotes the expression of C-Myc, Cyclin D1, and MMP-7, MMP-2, and MMP-9, and lead to many cellular events, including proliferation, invasion, and metastasis [35]. In the present study, we found HNPG caused the inhibition of proliferation, invasion, and metastasis, accompanied by the inactivation of  $\beta$ -catenin, which suggests that the wnt/ $\beta$ -catenin signal pathway is involved in the pharmacological effects of HNPG in inhibiting cell viability of JEC cells.

## Conclusions

HNPG demonstrated significant cytotoxic activity in human endometrial carcinoma JEC cells. HNPG inhibited proliferation, clone formation, invasion, and metastasis, and accumulated cell cycle in G1 phase *in vitro*. Simultaneously, decreased Rq and Ra increased Young's modulus and adhesion force in JEC cells. Additionally, HNPG inactivated the wnt/ $\beta$ -catenin signal pathway and downregulated the expression of  $\beta$ -catenin, C-Myc, Cyclin D1, MMP-2, MMP-7, and MMP-9. The present study not only detected the inhibiting effects of cell viability, but also elucidated the possible molecular mechanism of HNPG. In summary, HNPG shows marked cytotoxic activity in human endometrial carcinoma JEC cells via inactivating the wnt/ $\beta$ -catenin signal pathway, suggesting that HNPG may be a novel candidate for chemotherapeutic drugs. Subsequent studies will focus on investigating the metabolism of HNPG in experimental animal models, detecting its blood-drug concentration and its half-life and the adverse effects on the brain, heart, lung, liver, and kidney cells, and elucidate the possible molecular mechanism *in vivo*.

## Acknowledgements

The authors would like to thank Professor Manpeng Huo (the Medical School of Yanan University, Yanan, Shannxi, China) for his technical assistance.

## Conflicts of interests

None.

## References:

1. Ethier JL, Desautels DN, Templeton AJ et al: Is the neutrophil-to-lymphocyte ratio prognostic of survival outcomes in gynecologic cancers? A systematic review and meta-analysis. *Gynecol Oncol*, 2017; 145(3): 584–94
2. Kim SM, Rhee YH, Kim JS: The anticancer effects of radachlorin-mediated photodynamic therapy in the human endometrial adenocarcinoma cell line HEC-1-A. *Anticancer Res*, 2017; 37(11): 6251–58
3. Ding K, Yuan Y, Chong QY et al: Autocrine prolactin stimulates endometrial carcinoma growth and metastasis and reduces sensitivity to chemotherapy. *Endocrinology*, 2017; 158(6): 1595–611
4. Lester-Coll NH, Young MR, Park HS et al: Adjuvant therapy use and survival in stage II endometrial cancer. *Int J Gynecol Cancer*, 2017; 27(9): 1904–11
5. Zhong H, Liu H, Jiang Z: Genistein ameliorates fat accumulation through AMPK activation in fatty acid-induced BRL cells. *J Food Sci*, 2017; 82(11): 2719–25
6. Yousefi H, Karimi P, Alihemmati A et al: Therapeutic potential of genistein in ovariectomy-induced pancreatic injury in diabetic rats: The regulation of MAPK pathway and apoptosis. *Iran J Basic Med Sci*, 2017; 20(9): 1009–15
7. Chen Y, Cass SL, Kutty SK et al: Synthesis, biological evaluation and structure-activity relationship studies of isoflavene based mannich bases with potent anti-cancer activity. *Bioorg Med Chem Lett*, 2015; 25(22): 5377–83
8. Wang JH, Gao CJ, Meng LK: Study on the synthesis and antitumor effects of 5-hydroxy-4'-nitro-7-propionyloxy-isoflavone. *China Pharmacist*, 2012; 15(10): 1378–85
9. Jin YS, Liu CM, Wu QY et al: Design and synthesis of genistein derivatives 5-hydroxy-4'-nitro-7-substituted acyloxy isoflavone and their antitumor effects. *Acad J Mil Med Univ*, 2005; 26(2): 182–85
10. Wang H, Liu Z, Gou Y et al: Apoptosis and necrosis induced by novel realgar quantum dots in human endometrial cancer cells via endoplasmic reticulum stress signaling pathway. *Int J Nanomedicine*, 2015; 10: 5505–12
11. Li F, Liang A, Lv Y et al: MicroRNA-200c inhibits epithelial-mesenchymal transition by targeting the BMI-1 gene through the phospho-AKT pathway in endometrial carcinoma cells *in vitro*. *Med Sci Monit*, 2017; 23: 5139–49
12. Krishnamurthy N, Kurzrock R: Targeting the wnt/beta-catenin pathway in cancer: Update on effectors and inhibitors. *Cancer Treat Rev*, 2018; 62: 50–60
13. Shanmugapriya S, Subramanian P, Kanimozhi S: Geraniol inhibits endometrial carcinoma via downregulating oncogenes and upregulating tumour suppressor genes. *Indian J Clin Biochem*, 2017; 32(2): 214–19
14. Eritja N, Yeramian A, Chen BJ et al: Endometrial carcinoma: Specific targeted pathways. *Adv Exp Med Biol*, 2017; 943: 149–207
15. Liu Y, Patel L, Mills GB et al: Clinical significance of CTNNB1 mutation and wnt pathway activation in endometrioid endometrial carcinoma. *J Natl Cancer Inst*, 2014; 106(9): pii: dju245
16. Chen H, Wang Y, Xue F: Expression and the clinical significance of wnt10a and wnt10b in endometrial cancer are associated with the wnt/ $\beta$ -catenin pathway. *Oncol Rep*, 2013; 29(2): 507–14
17. Zhao Y, Yang Y, Trovik J et al: A novel wnt regulatory axis in endometrioid endometrial cancer. *Cancer Res*, 2014; 74(18): 5103–17
18. Ketelboeter LM, Bardy SL: Methods to inhibit bacterial pyomelanin production and determine the corresponding increase in sensitivity to oxidative stress. *J Vis Exp*, 2015; (102): e53105
19. Lei KF, Kao CH, Tsang NM: High throughput and automatic colony formation assay based on impedance measurement technique. *Anal Bioanal Chem*, 2017; 409(12): 3271–77
20. Shapiro CL, Moriarty JP, Dusetzina S et al: Cost-effectiveness analysis of monthly zoledronic acid, zoledronic acid every 3 months, and monthly denosumab in women with breast cancer and skeletal metastases: CALGB 70604 (Alliance). *J Clin Oncol*, 2017; 35(35): 3949–55
21. Chen DY, See LC, Liu JR et al: Risk of cardiovascular ischemic events after surgical castration and gonadotropin-releasing hormone agonist therapy for prostate cancer: A nationwide cohort study. *J Clin Oncol*, 2017; 35(32): 3697–705
22. Ono M, Ejima K, Higuchi T et al: Equol enhances apoptosis-inducing activity of Genistein by increasing bax/bcl-xl expression ratio in MCF-7 human breast cancer cells. *Nutr Cancer*, 2017; 69(8): 1300–7
23. Azevedo C, Correia-Branco A, Araújo JR et al: The chemopreventive effect of the dietary compound kaempferol on the MCF-7 human breast cancer cell line is dependent on inhibition of glucose cellular uptake. *Nutr Cancer*, 2015; 67(3): 504–13
24. Latocha M, Płonka J, Kuśmierz D et al: Transcriptional activity of genes encoding MMPs and TIMPs in breast cancer cells treated by Genistein and in normal cancer-associated fibroblasts – *in vitro* studies. *Acta Pol Pharm*, 2014; 71(6): 1095–102
25. Kim LH, Khadka S, Shin JA et al: Nitidine chloride acts as an apoptosis inducer in human oral cancer cells and a nude mouse xenograft model via inhibition of STAT3. *Oncotarget*, 2017; 8(53): 91306–15
26. So E, Kim J, Joo S et al: Association of dietary patterns with overweight risk and all-cause mortality in children with cancer. *Nutr Res Pract*, 2017; 11(6): 492–99
27. Kim CJ, Terado T, Tambe Y et al: Anti-oncogenic activities of cyclin D1b siRNA on human bladder cancer cells via induction of apoptosis and suppression of cancer cell stemness and invasiveness. *Int J Oncol*, 2018; 52(1): 231–40
28. Morita S, Nakamaru Y, Homma A et al: Expression of p53, p16, cyclin D1, epidermal growth factor receptor and Notch1 in patients with temporal bone squamous cell carcinoma. *Int J Clin Oncol*, 2017; 22(1): 181–89
29. Rossi HS, Koho NM, Ilves M et al: Expression of extracellular matrix metalloproteinase inducer and matrix metalloproteinase-2 and -9 in horses with chronic airway inflammation. *Am J Vet Res*, 2017; 78(11): 1329–37
30. Taniguchi M, Matsuura K, Nakamura R et al: MMP-7 cleaves amyloid  $\beta$  fragment peptides and copper ion inhibits the degradation. *Biometals*, 2017; 30(5): 797–807
31. Cascione M, De Matteis V, Toma CC et al: Morphomechanical and structural changes induced by ROCK inhibitor in breast cancer cells. *Exp Cell Res*, 2017; 360(2): 303–9
32. Meng F, Saxena S, Liu Y et al: The phospho-caveolin-1 scaffolding domain dampens force fluctuations in focal adhesions and promotes cancer cell migration. *Mol Biol Cell*, 2017; 28(16): 2190–201
33. Laurito T, Sueiras V, Fernandez N et al: Assessment of micro-mechanical variations in experimental arteriovenous fistulae using atomic force microscopy. *J Vasc Access*, 2016; 17(3): 279–83
34. Joo HJ, Jeong KH, Kim JE, Kang H: Various wavelengths of light-emitting diode light regulate the proliferation of human dermal papilla cells and hair follicles via wnt/ $\beta$ -catenin and the extracellular signal-regulated kinase pathways. *Ann Dermatol*, 2017; 29(6): 747–54
35. Kasprzak A, Rogacki K, Adamek A et al: Tissue expression of  $\beta$ -catenin and E- and N-cadherins in chronic hepatitis C and hepatocellular carcinoma. *Arch Med Sci*, 2017; 13(6): 1269–80